Hierarchical Spatial-temporal Event Modeling and Optimal Regulation of Integrated Energy Cyber-physical Systems

Yi Yang, Ping Tang, Can Wang, Nan Yang, and Zhuoli Zhao

***Abstract*—The integrated energy cyber-physical system (IECPS), a typical cyber-physical system (CPS), demonstrates tight interaction between cyber and physical spaces across time and space, exhibiting inherent spatial-temporal properties. Effective IECPS modeling requires the simultaneous consideration of both temporal and spatial properties, which remains a significant challenge. This paper proposes a hierarchical spatial-temporal event modeling method for IECPS based on hybrid automata (HA). Different event model layers are defined, representing events as functions of attributes, time, and space, with attributes characterized by system states. An integration method for multi-layer events is introduced, enabling accurate reflection of the system spatial-temporal characteristics and the current operating state of energy units. The modeling is applied to the optimal regulation of IECPS. Numerical simulations demonstrate that the proposed HA-based modeling method achieves precise regulation of IECPS while reducing system operating costs.**

***Index Terms*—Cyber-physical system (CPS), hybrid automata, integrated energy cyber-physical system (IECPS), operating cost, event modeling.**

I. Introduction

THE large-scale integration of renewable energy sources (RESs) into the integrated energy system (IES) has significantly intensified the coupling between multiple energy subsystems [1], [2]. To maximize the RES utilization and enhance the operational economy of IES, it is essential to conduct coordinated and intelligent control of individual subsystems [3], [4]. Cyber-physical system (CPS) offers an effective approach to this challenge. By tightly integrating information technologies (such as communication, computation, and control) with physical infrastructures (including electricity, heating, and natural gas), a CPS enables real-time sensing, dynamic optimization, and intelligent decision-making [5], [6]. This integration supports the coordinated operation of IES components. With the rapid advancement of Energy Internet and ongoing digital transformation, IESs are evolving into complex CPS structures, collectively referred to as integrated energy cyber-physical systems (IECPSs). Addressing the challenges posed by the deep integration and coordinated control of cyber and physical subsystems in the IECPS necessitates the robust CPS-based modeling methods.

Recent research on IECPS modeling has concentrated on four key areas: system security, interaction analysis, resilience assessment, and optimal regulation. In system security modeling, [7] developed an integrated modeling framework and operating state analysis under coordinated attacks, contributing new insights into system protection. Reference [8] introduced a method for modeling risk propagation and loss causation in key nodes of coupled cyber-physical power networks, offering tools for identifying and securing critical components. Reference [9] examined the security of coupled transportation and cyber-physical power system using static Bayesian game theory, laying the theoretical groundwork for defense strategies in multi-system environments. Reference [10] analyzed the robustness of weakly-coupled cyber-physical power systems under multi-stage attacks, elucidating the relationship between system vulnerability and attack patterns. For interaction modeling, [11] proposed a comprehensive model to assess the effects of cyber-physical interactions in Energy Internet systems, supporting collaborative optimization efforts. Reference [12] introduced a simulation control method tailored for IECPS modeling, enhancing system design and analysis. Reference [13] applied graph convolutional networks to identify critical components in cascading failures within CPS, providing insights for reliability improvement. Reference [14] developed a reliability assessment method considering multi-state independent components, offering an alternative approach for system reliability analysis. Reference [15] presented a hybrid model to examine disturbance propagation in CPS, contributing to system stability analysis. For resilience modeling, [16] provided a systematic review of resilience metrics and modeling techniques for

Manuscript received: December 2, 2024; revised: March 4, 2025; accepted: May 30, 2025. Date of CrossCheck: May 30, 2025. Date of online publication: June 19, 2025.

This work was supported in part by the Hubei Provincial Department of Education Young Talent Program (No. Q20231208), in part by the Hubei Provincial Natural Science Foundation Program (No. 2025AFB085), and in part by the Three Gorges University Talent Research Initiation Fund (No. Z2023404).

Y. Yang (corresponding author), P. Tang, C. Wang, and N. Yang are with the Hubei Provincial Key Laboratory for Operation and Control of Cascaded Hydropower Station, College of Electrical Engineering and New Energy, China Three Gorges University, Yichang 443002, China (e-mail: epyyang@163.com; yyang_151@yeah.net; xfcancan@163.com; ynyyayy@ctgu.edu.cn).

Z. Zhao is with the Department of Electrical Engineering, School of Automation, Guangdong University of Technology, Guangzhou 510006, China (e-mail: zhuoli.zhao@gdut.edu.cn).

DOI: 10.35833/MPCE.2024.001263

CPS, outlining future resilience research directions. Reference [17] introduced a resilience assessment approach accounting for cyber-attacks, facilitating quantitative evaluation of system robustness. Reference [18] proposed a sequential restoration strategy incorporating electricity-gas coupling characteristics for post-disaster recovery, supporting rapid system restoration. Reference [19] developed a resilience enhancement method using Gaussian process-based prior information, introducing a novel design strategy for resilience. In the optimal regulation modeling, [20] formulated a multi-objective and multi-constraint optimization model for CPS incorporating RES and electric vehicles, targeting low-carbon and economically efficient operations. Reference [21] proposed an adequacy assessment approach for multi-microgrid distributed systems considering the role of distributed generation, which supports the system planning and operation. Reference [22] addressed the reliability of short-term load forecasting in CPS using adaptive denoising, offering data support for operational control.

Despite significant progress in IECPS modeling, several key challenges remain.

1) IECPS exhibits both continuous dynamic and discrete behaviors during operation. Existing IECPS models predominantly emphasize continuous dynamics, lacking a unified framework that concurrently addresses discrete and continuous system characteristics.

2) Existing IECPS models primarily focus on interactions between cyber and physical domains without adequately capturing the spatial-temporal nature of CPS. CPS links the cyber and physical domains through computation, communication, and control, necessitating synchronized interactions across time and space. Simultaneously, CPS introduces additional complexity by requiring accurate representation of dynamics, timeliness, and concurrency, collectively referred to as spatial-temporal challenges. These challenges can be addressed by integrating temporal and spatial properties to enhance the performance and fidelity of IECPS models.

Spatial-temporal properties in CPS are often manifested through events, as CPS is fundamentally event-driven [23]. Given the efficacy of events in representing spatial-temporal properties, this study adopts an event modeling method for CPS. Previous studies [24] - [26] have explored CPS event models; however, these models generally incorporate only temporal features and omit spatial attributes and system dynamics, particularly the state transition processes. To address these gaps, a CPS event model that integrates both temporal and spatial properties is proposed. This model is applied to the optimal regulation of IECPS. The main contributions of this paper are summarized as follows.

1) A state transition model of energy units in IECPS is developed using hybrid automata (HA), enabling transitions between operating states based on system conditions. This model provides a unified representation of both discrete and continuous system behaviors.

2) A hierarchical spatial-temporal event modeling method for IECPS is proposed, and the corresponding models for each layer are constructed. The HA-based state transition model is embedded within these events, capturing both spatial-temporal properties and state transitions of energy units.

3) An integration method for multi-layer event models is introduced, enabling coordinated decision-making across IECPS layers. This method supports optimized system operation and cost reduction.

The structure and state transition model of IECPS are presented in Section II. Section III details the spatial-temporal event model for IECPS. Section IV discusses case studies. Conclusions are provided in Section V.

II. Structure and State Transition Model of IECPS

A. Typical Structure of IECPS

The typical structure of IECPS is illustrated in Fig. 1, which comprises two main components: the cyber system and physical system.

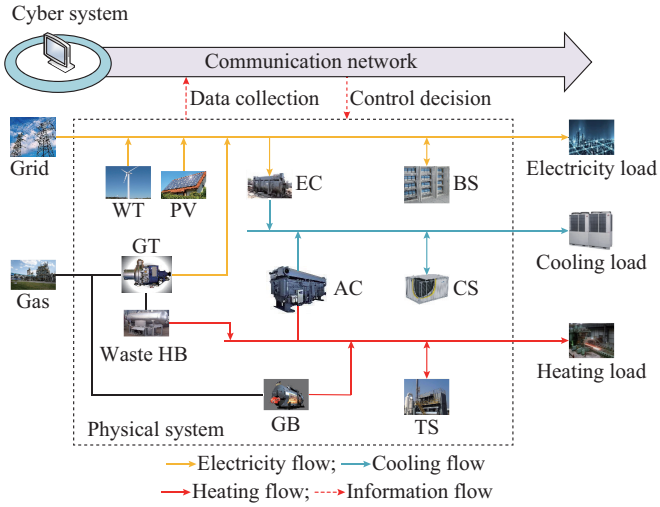

Fig. 1. Typical structure of IECPS.

The physical components of IECPS include energy production units (EPUs), energy conversion units (ECUs), energy storage units (ESUs), and energy consumption units (ECSUs). EPUs serve as energy sources and primarily include renewable energy technologies such as photovoltaic (PV) systems and wind turbines (WTs), as well as power supplied from the power grid and natural gas networks. ECUs facilitate the conversion between various forms of energy and include devices such as gas turbine (GT), gas boiler (GB), waste heat boiler (HB), electric chiller (EC), and absorption chiller (AC). For instance, EC converts electricity energy into cooling energy, while AC utilizes heating energy for refrigeration purposes. ESUs consist of battery storage (BS), thermal storage (TS), and cold storage (CS) systems, each designed to store specific energy forms. ECSUs represent the end-use energy demands and encompass electricity, heating, and cooling loads. Detailed models of these energy units are available in [27] and are not repeated here.

The cyber component comprises data acquisition and control devices for the energy units, distributed computing systems, decision-making and control modules, and the communication infrastructure connecting all cyber elements. Functioning as the control center of IECPS, the cyber system is

responsible for monitoring data, executing optimization tasks, analyzing information received from the physical system, and generating the corresponding control commands.

B. Principle of HA

The IECPS exhibits both continuous and discrete dynamic behaviors during operation. Conventional modeling methods, which focus solely on either discrete or continuous dynamics, are insufficient to capture this hybrid behavior. To address this, HA is adopted for modeling.

HA extends the classical finite state machine (FSM) framework by incorporating continuous variables and differential equations to describe their evolution. The HA model is defined by the following tuple [28]:

$$H=\{S,X,f,Init,\delta,G\} \tag{1}$$

where $S=\{s_1,s_2,...,s_n\}$ is the set of operating states s_i of the system, and n is the number of total operating states; X is the set of continuous variables of the system; f is the characteristic of the system state variables changing with time when the system is in the operating state s_i; *Init* is the set of initial states of the system; δ is the state transition function, describing how the operating state of the system changes; and G is the condition for the system to transition between different states.

In this context, the continuous dynamics of energy unit outputs are represented by f, while the discrete state transitions are described by δ.

A typical HA consists of the following components: ① current state; ② condition (also called the event, which triggers a state transition of the system when G is satisfied); ③ action (the state transition performed by the system after G is satisfied); and ④ next state (the state that the system will transition).

HAs are often visualized as directed graphs. An example with three states is shown in Fig. 2, where each circle represents a discrete state; each arrow indicates transitions between states, with the starting point denoting the current state and the ending point indicating the next state; and the guard condition $G(i,j)$ enabling the transition is labeled along the corresponding edge.

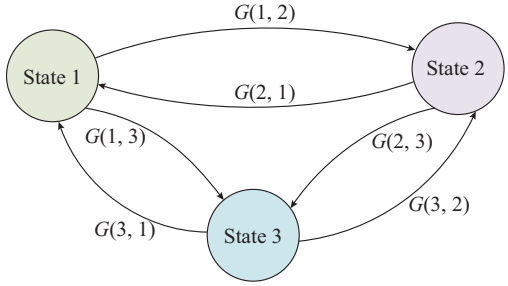

Fig. 2. Graphical representation of an HA.

C. HA-based State Transition Model of IECPS

This subsection first presents the HA-based state transition model of an energy unit, followed by the development of the state transition model for IECPS.

1) State Transition Model of Energy Unit

Taking the BS as an example, the charging/discharging model is formulated as:

$$\begin{cases} SOC(t+1)=SOC(t)+\dfrac{\eta_{bs,c}P_{bs,c}(t)\Delta t}{S_{bs}}-\dfrac{P_{bs,d}(t)\Delta t}{\eta_{bs,d}S_{bs}} \\ SOC_{\min}\le SOC(t)\le SOC_{\max} \\ SOC_0=0.5\cdot SOC_{\max} \\ 0\le P_{bs,c}(t)\le v_{bs,c}(t)P_{bs,c,\max} \\ 0\le P_{bs,d}(t)\le v_{bs,d}(t)P_{bs,d,\max} \\ v_{bs,c}(t)+v_{bs,d}(t)\le 1 \\ \eta_{\min}\le \eta_{bs,c}(t) \\ \eta_{bs,d}\le \eta_{\max}(t) \\ P_{bs,c}(t)+P_{bs,d}(t)\le \dfrac{Q_{\max}}{h_c} \end{cases} \tag{2}$$

where S_{bs} is the rated capacity of BS; $\eta_{bs,c}$ and $\eta_{bs,d}$ are the charging and discharging efficiencies of BS, respectively; $\eta_{\max}$ and $\eta_{\min}$ are the upper and lower bounds of efficiency, respectively; $P_{bs,c}(t)$ and $P_{bs,d}(t)$ are the charging and discharging power of BS, respectively; $P_{bs,c,\max}$ and $P_{bs,d,\max}$ are the maximum charging and discharging power of BS, respectively; $SOC_{\max}$ and $SOC_{\min}$ are the maximum and minimum state-of-charge (SOC) limits, respectively; SOC_0 is the initial SOC; $v_{bs,c}(t)$ and $v_{bs,d}(t)$ are the binary variables representing the charging and discharging states, respectively; $Q_{\max}$ is the maximum thermal dissipation; and h_c is the thermal dissipation coefficient, representing the heat generated per unit of power.

The HA-based state transition model of BS is illustrated in Fig. 3, which enables state transitions in response to changes in the external environment or control commands. Meanwhile, the state equations for each energy unit are updated, ensuring an integrated representation of discrete logic switching and continuous dynamic adjustment.

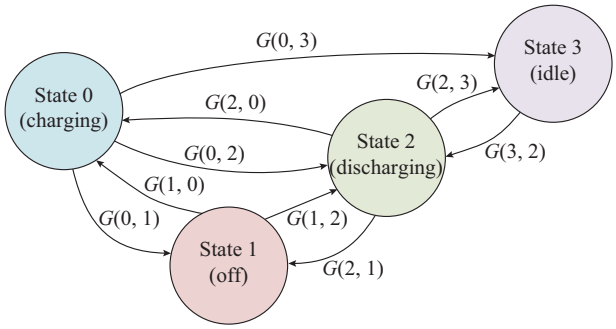

Fig. 3. HA-based state transition model of BS.

2) State Transition Model of IECPS

An HA-based dynamic model is established to characterize the IECPS behavior under various operating states. These states result from different combinations of operational conditions across energy units, as shown by n operating states in Fig. 4, where each block represents a distinct operating state of IECPS, and MPPT is short for maximum power point tracking.

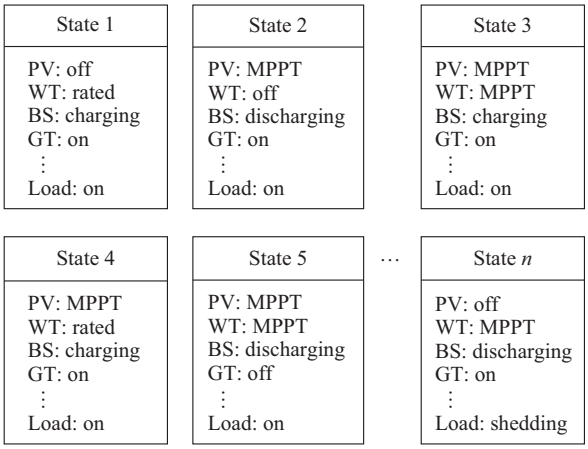

Fig. 4. n operating states of IECPS.

The IECPS is composed of three interdependent subsystems: electricity, heating, and cooling subsystems. They are interconnected via ECUs. The system dynamics in each state are represented using the following state-space formulation:

$$\begin{cases} \boldsymbol{x}(t+1)=\boldsymbol{A}\boldsymbol{x}(t)+\boldsymbol{B}\boldsymbol{u}(t)+\boldsymbol{E}\boldsymbol{d}(t)+\boldsymbol{W}\boldsymbol{r}(t) \\ \boldsymbol{x}(t)=[x_e(t), x_h(t), x_c(t)]^{\mathrm{T}} \end{cases} \tag{3}$$

where $\boldsymbol{x}(t)$, $\boldsymbol{u}(t)$, $\boldsymbol{d}(t)$, and $\boldsymbol{r}(t)$ are the vectors of state variables, control inputs, disturbances, and coupling variables, respectively, and $\boldsymbol{A}$, $\boldsymbol{B}$, $\boldsymbol{E}$, and $\boldsymbol{W}$ are the matrices representing the dynamics of each component. Based on the subsystem response characteristics, the state variable $\boldsymbol{x}(t)$ is divided into three groups: $x_e(t)$, $x_h(t)$, and $x_c(t)$, which correspond to the electricity, heating, and cooling subsystems, respectively. The detailed derivation is provided in Supplementary Material A.

Because of the dynamic nature of subsystem interaction, the transitions between different states of IECPS depend on evolving system conditions. The HA-based state transition model of IECPS is shown in Fig. 5.

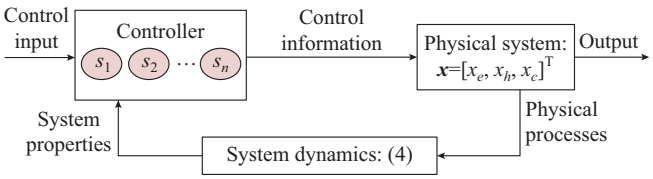

Fig. 5. HA-based state transition model of IECPS.

The system dynamic behaviors across operating states are represented as:

$$\boldsymbol{x}(t+1)=\boldsymbol{A}_{s(t)}\boldsymbol{x}(t)+\boldsymbol{B}_{s(t)}\boldsymbol{u}(t)+\boldsymbol{E}_{s(t)}\boldsymbol{d}(t)+\boldsymbol{W}_{s(t)}\boldsymbol{r}(t) \tag{4}$$

where $s(t)=s_j$ is the current state, and $s_j \in S$; and $\boldsymbol{A}_{s(t)}$, $\boldsymbol{B}_{s(t)}$, $\boldsymbol{E}_{s(t)}$, and $\boldsymbol{W}_{s(t)}$ are the matrices describing the system dynamics under state $s(t)$.

III. Spatial-temporal Event Model for IECPS

This section presents a three-layer modeling framework for IECPS and defines the concept of spatial-temporal events. A spatial-temporal event model is then developed for IECPS.

A. Three-layer Modeling Framework for IECPS

The three-layer modeling framework for IECPS comprises the physical layer, integration layer, and decision layer, as illustrated in Fig. 6, where the elements e_{phy}, e_{pc}, e_{cyb}, and e_{con} represent the physical events, cyber-physical events, cyber events, and control events, respectively.

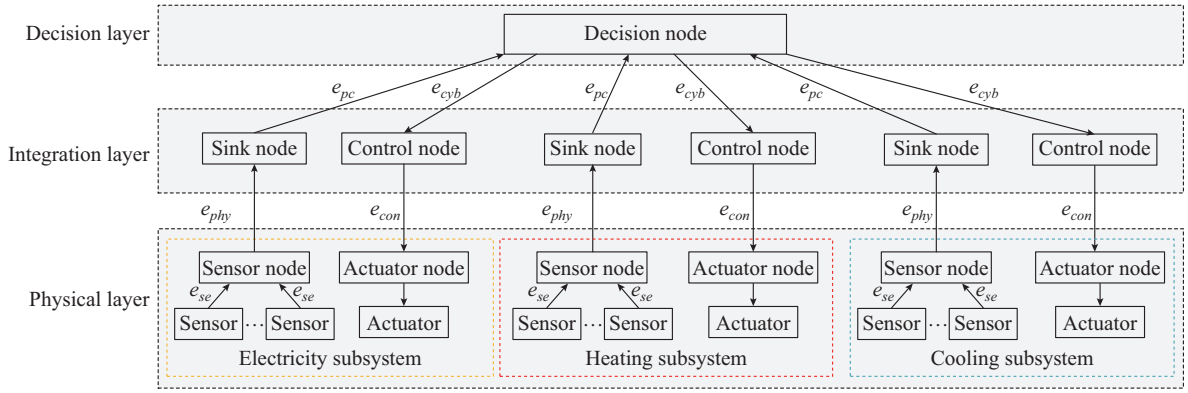

Fig. 6. Three-layer modeling framework for IECPS

1) Physical layer: this layer consists of physical components such as sensors, actuators, and energy units. To accommodate different response characteristics of energy units, the physical layer is divided into electricity, heating, and cooling subsystems. The energy units within each subsystem are modeled using HA and are uploaded to the integration layer in the form of events.

2) Integration layer: this layer includes multiple sink and control nodes. Sink nodes aggregate events transmitted from sensor nodes in the physical layer to generate cyber-physical events, which are forwarded to the decision layer to support decision-making. Control nodes interpret cyber events received from the decision layer, generate the corresponding control events, and dispatch them to actuators in the physical layer for execution.

3) Decision layer: this layer processes cyber-physical events received from sink nodes in the integration layer and generates cyber events representing decision objectives. These objectives are sent to the integration layer and may include goals such as minimizing the total operation cost or

maximizing the use of renewable energy.

The modeling framework shown in Fig. 6 enables the representation of state changes in physical devices. It accommodates the spatial-temporal distribution and heterogeneity characteristic of CPS, exhibiting the following advantages. ① It supports event-based operations in distributed and heterogeneous CPS environments. ② It captures system dynamics by modeling transitions in physical device states. ③ It integrates spatial and temporal attributes to formulate spatial-temporal properties.

B. Spatial-temporal Event Definitions

CPS requires synchronized interactions between the cyberspace and physical domain across both time and space. These interactions are typically governed by events, which describe the states of one or more entities in cyberspace or the physical domain based on specified properties, time, and location [29]-[31]. The events can be defined as:

$$E(type_h)(ID_h,\ SR_h)(t_h, d_h, s_h\{s_1, s_2, ..., s_n\}) \tag{5}$$

where $E(type_h)$ is the event type (e.g., sensor event or physical event); ID_h is the event node identifier; SR_h corresponds to the sensor type associated with ID_h; t_h is the event occurrence time; d_h is the event location, which may fall within the electricity, heating, or cooling subsystems of the IECPS; and $s_h\{s_1, s_2, ..., s_n\}$ is the set of multi-dimensional properties associated with the event.

C. Spatial-temporal Event Modeling for IECPS

1) Physical Layer

The physical layer comprises multiple sensors, each designed to detect a single physical property. For example, a PV sensor detects only light intensity, while a WT sensor measures only wind speed. To facilitate the efficient management, multiple sensors are integrated into a single sensor node. Sensor nodes are classified into three categories: electricity, heating, and cooling sensor nodes. Sensors monitoring devices in electricity subsystem (e. g., PV panels and WTs) are grouped into electricity sensor nodes. Sensors monitoring devices in heating subsystem (e.g., TS and HBs) and cooling subsystem (e. g., air conditioners and CS units) are grouped into heating and cooling sensor nodes, respectively, as illustrated in Fig. 7. To enhance the accuracy and robustness, multiple sensor nodes are typically deployed in the physical layer.

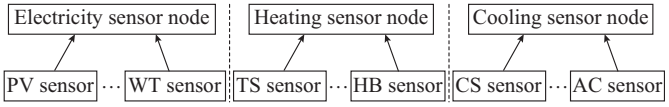

Fig. 7. Sensor nodes in physical layer.

When the operating state of an energy unit changes, the sensors detect this change and generate a sensor event, denoted as e_{se}, which is then uploaded to the system. The sensor event is formally defined as:

$$E(type_{se})(ID_{k,m}, SR_{se})(t_{se}, d_{se}, s_{se}\{s_1, s_2, ..., s_n\}) \tag{6}$$

where $E(type_{se})$ is the sensor event index; $ID_{k,m}$ is the sensor node identifier, with $k = e, h, c$ representing electricity, heating, cooling sensor nodes, respectively and $m = 1, 2, \ldots$ representing the No. of node; SR_{se} corresponds to the sensor type associated with $ID_{k,m}$, e. g., it can be the sensor that senses light intensity and wind speed; t_{se} and d_{se} are the occurrence time and location of sensor event, respectively; and $s_{se}\{s_1, s_2, \ldots, s_n\}$ is the set of multi-dimensional properties of sensor event, with a default value of 0 for each component. When the value of one component exceeds a certain threshold, it is then set to an integer, representing the operating state of energy unit. Here, n corresponds to the number of sensors integrated into the node.

For example, considering the electricity sensor node 1, this node integrates a PV sensor, a WT sensor, a BS sensor, and a sensor measuring power exchanged between the grid and the IECPS, represented by SR_{sePV}, SR_{seWT}, SR_{seBS}, and SR_{sePG}, respectively. If the PV sensor detects light intensity exceeding the defined threshold, the first component of s_{se} is set to be 1, while the remaining components retain their default value of 0, as each sensor monitors only one property. The resulting sensor event is expressed as:

$$E(type_{se})(ID_{e,1}, SR_{sePV})(0.5, d_e, s_{se}\{1, 0, 0, 0\}) \tag{7}$$

Formula (7) indicates that the sensor event originates from the PV sensor within electricity sensor node 1. The event in the electricity subsystem d_e occurs at $t_{se} = 0.5$ s and reflects that the PV unit is operating in the MPPT state.

The sensor events from the WT sensor, BS sensor, and the sensor measuring power exchanged between the grid and the IECPS are assumed to follow the form presented in (8).

$$\begin{cases} E(type_{se})(ID_{e,1}, SR_{seWT})(0.5, d_e, s_{se}\{0, 1, 0, 0\}) \\ E(type_{se})(ID_{e,1}, SR_{seBS})(0.8, d_e, s_{se}\{0, 0, 3, 0\}) \\ E(type_{se})(ID_{e,1}, SR_{sePG})(0.8, d_e, s_{se}\{0, 0, 0, 1\}) \end{cases} \tag{8}$$

Multiple sensors are installed on the electricity sensor node 1, each generating distinct events. The physical event e_{phy} results from integrating these various sensor events received by electricity sensor node 1, as defined in:

$$E(type_{phy})(ID_{e,1})(t_{phy}, d_{phy}, s_{phy}\{s_1, s_2, \ldots, s_n\}) \tag{9}$$

where $E(type_{phy})$ is the physical event index; t_{phy} and d_{phy} are the occurrence time and location of physical event, respectively; and $s_{phy}\{s_1, s_2, \ldots, s_n\}$ is the set of multi-dimensional properties of physical event.

It is critical to develop a method for integrating different events. This paper implements an HA for this purpose. To clarify the relationship between HA and event modeling, define e_{sePV}, e_{seWT}, e_{seBS}, and e_{sePG} as the sensor events from the PV, WT, BS, and the sensor measuring power exchanged between the grid and IECPS, respectively. The multi-element tuple representation of HA is extended as:

$$H = \{S, X, f, Init, I_h, O_h, \delta, G\} \tag{10}$$

where I_h is the HA input, i.e., the sensor event e_{se}; O_h is the HA output, i.e., the physical event e_{phy}; and δ is expressed in (11), which integrates all sensor events generated simultaneously by sensors on the node into the physical event e_{phy}.

$$\begin{cases} O_h=\delta(I_h)=e_{phy} \\ I_h=(e_{sePV},e_{seWT},e_{seBS},e_{sePG}) \\ \delta(e_{sePV},e_{seWT},e_{seBS},e_{sePG})=(t_{phy},d_{phy},s_{phy}) \\ t_{phy}=AVG(t_{sePV},t_{seWT},t_{seBS},t_{sePG}) \\ \{d_{phy}\}=\{d_{sePV},d_{seWT},d_{seBS},d_{sePG}\} \\ s_{phy}=s_{sePV}\cup s_{seWT}\cup s_{seBS}\cup s_{sePG} \end{cases} \tag{11}$$

where the occurrence time t_{sePV}, t_{seWT}, t_{seBS}, and t_{sePG} of different sensor events is averaged using function $AVG(\cdot)$ to yield t_{phy}; the occurrence locations d_{sePV}, d_{seWT}, d_{seBS}, and d_{sePG} of different sensor events are combined into the union set, defining d_{phy}; and the sets s_{sePV}, s_{seWT}, s_{seBS}, and s_{sePG} of different sensor events are combined into the union set, forming s_{phy}. Because all sensors are integrated within the same sensor node, their locations coincide, i.e., $d_{phy}=d_e$.

The physical event obtained by electricity sensor node 1 is expressed as:

$$E(type_{phy})(ID_{e,1})(1.3,d_e,s_{phy}\{1,1,3,1\}) \tag{12}$$

Formula (12) describes the PV operating in the MPPT mode, the WT at the rated power, the BS in the idle state, and the IECPS purchasing electricity from power grid. The operation of sensor nodes for heating and cooling subsystems mirrors for electricity subsystem and hence is omitted here.

2) Integration Layer

The integration layer performs the following main tasks.

1) Monitor and record the operating state information of various devices in the physical layer, including both discrete and continuous data.

2) Integrate and process e_{phy} uploaded by the physical layer to generate cyber-physical events e_{pc}, which are then uploaded to the decision layer.

3) Receive decision objectives from the decision layer and convert them into control objectives to guide operations in the physical layer.

This layer is modeled using a multi-element tuple, as shown in (13).

$$I=\{D,F_D,F_{ctr},A\} \tag{13}$$

where D, F_D, F_{ctr}, and A are introduced as follows.

① D is the data record in the integration layer that stores the operating state data of the physical layer:

$$\begin{cases} D=\{D_1,D_2,...,D_N\} \\ D_i=\{q_i,x_i\} \end{cases} \tag{14}$$

where N is the number of energy units in the physical layer; and D_i is the state data set of energy unit i, which includes discrete state data q_i and continuous state data x_i. The discrete state data q_i primarily indicates the operating states of energy unit, while the continuous state data x_i includes parameters such as the output power and stored energy of ESUs.

② F_D is the state data monitoring and recording function, which is responsible for tracking the operating states of energy units in the physical layer and recording the information into D.

$$F_D:[q,x]\rightarrow D \tag{15}$$

③ F_{ctr} is the control function in the integration layer that generates control commands $C(t)$ for energy units. This function relies on the current operating states of energy units and the decision objectives received from decision layer.

$$F_{ctr}:D\rightarrow C(t) \tag{16}$$

④ A is the set of interfaces for integration layer. Since the interaction between layers occurs via event transmission, A includes interface A_s with the decision layer and interface A_o with the physical layer.

$$\begin{cases} A=\{A_s,A_o\} \\ A_s=\{f_{sup},f_{sdown}\} \\ A_o=\{f_{oup},f_{odown}\} \end{cases} \tag{17}$$

where the function f_{odown} sends control events e_{con}, generated by the control node, to the corresponding actuators in the physical layer to execute control commands; the function f_{oup} uploads physical events e_{phy} generated by the physical layer to the sink node in the integration layer, in which the physical events are integrated and converted into cyber-physical events e_{pc}; and the function f_{sup} uploads physical events e_{pc} to the decision layer, at which the analysis produces cyber events e_{cyb} that are sent back to the integration layer through f_{sdown}. The cyber-physical event is defined as:

$$E(type_{pc})(ID_{pc,k})(t_{pc},d_{pc},s_{pc}\{s_1,s_2,...,s_n\}) \tag{18}$$

where $E(type_{pc})$ is the cyber-physical event index; $ID_{pc,k}$ is the sink node identifier; t_{pc} and d_{pc} are the occurrence time and location of cyber-physical event, respectively; and $s_{pc}\{s_1,s_2,...,s_n\}$ is the set of multi-dimensional properties of cyber-physical event. Multiple electricity, heating, and cooling sensor nodes are typically deployed in the physical layer to enhance the system accuracy and robustness. Therefore, the sink node receives multiple physical events e_{phy} uploaded simultaneously by the sensor nodes under its management, as illustrated in Fig. 8.

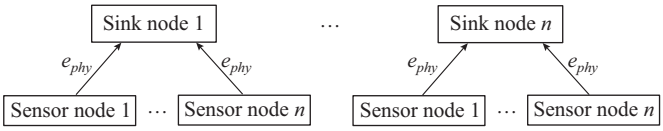

Fig. 8. Sink nodes in integration layer.

Because physical events are transmitted through a communication network, delays can occur due to network congestion or other issues. Therefore, when integrating the received physical events, the sink node applies a timeout judgment. If the delay of any physical event exceeds a preset threshold, the physical event is considered invalid. This mechanism filters out the delayed events caused by network failure or congestion, preventing them from affecting system decisions and performance.

The timeout judgment rule assumes that each sink node has a local time t_{sink} and a maximum allowable delay t_{delay}. When a physical event satisfies $|t_{phy}-t_{sink}|\le t_{delay}$, the physical event is considered valid; otherwise, it is discarded.

For example, consider sink node 1 managing two electricity sensor nodes. If the physical event e_{phy} uploaded by sensor node 2 experiences severe delay due to network failure, the

integrated cyber-physical event obtained by sink node 1 is expressed as:

$$E(type_{pc})(ID_{pc,1})(1.3, d_e, s_{pc}\{0, 1, 3, 1\}) \tag{19}$$

The function f_{sup} uploads the cyber-physical event e_{pc} generated by the integration layer to the decision node in the decision layer. The decision node processes the cyber-physical event e_{pc} and converts it into the cyber event e_{cyb}. The function f_{odown} sends the cyber event e_{cyb} generated by the decision layer to the control node in the integration layer. The control node processes the control event e_{con}, and converts it into the cyber event e_{cyb}, representing the control objective. The definitions of cyber event e_{cyb} and control event e_{con} are detailed in the decision layer.

After all sink nodes in the integration layer complete the integration of physical events e_{phy} uploaded from the physical layer, multiple sets of operating states for the electricity, heating, and cooling subsystems are obtained. By using the electricity subsystem as an example, with PV and WT as non-dispatchable energy sources and assuming the load remains continuously on, a total of 16 dispatchable operating states arise from combinations of the energy units in electricity subsystem, as illustrated in Fig. 9, where each block represents one operating state of the electricity subsystem.

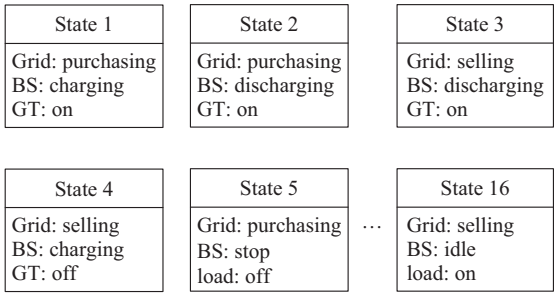

Fig. 9. A total of 16 dispatchable operating states.

The transition process of these 16 operating states during operation according to system requirements is shown in Fig. 10.

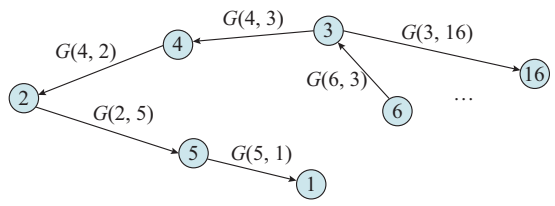

Fig. 10. Transition process of 16 operating states.

Adjusting $G(i,j)$ enables the electricity subsystem to operate in the desired states to fulfill decision objectives from the decision layer. The integrated operating states of the heating and cooling subsystems follow a similar pattern and are not further described.

3) Decision Layer

The decision layer further integrates the physical events e_{pc} from the integration layer to generate cyber events e_{cyb} (decision objective), which is transmitted back to the integration layer. The decision objective is to minimize the daily operating cost F_r of the IECPS, which is expressed as:

$$\min F_{\mathrm{r}} = \sum_{t=1}^{T}(c_{eb,t}P_{gb,t} - c_{es,t}P_{gs,t} + c_{pg,t}P_{gas,t})\Delta t \tag{20}$$

where $c_{eb,t}$ and $c_{es,t}$ are the purchased and sold electricity prices at time t, respectively; $P_{gb,t}$ and $P_{gs,t}$ are the purchased and sold power at time t, respectively; $c_{pg,t}$ is the natural gas price at time t; $P_{gas,t}$ is the amount of natural gas purchased at time t; Δt is the time scale; and T is the scheduling period. In this part, $\Delta t = 1$ hour, and $T = 24$ hours. Constraints include power balance (see Supplementary Material A), energy unit output, and electricity purchase constraints.

1) Energy unit output constraints

$$\begin{cases} P_{i,\min} \le P_i(t) \le P_{i,\max} \\ H_{i,\min} \le H_i(t) \le H_{i,\max} \\ C_{i,\min} \le C_i(t) \le C_{i,\max} \end{cases} \tag{21}$$

where $P_{i,\min}$ and $P_{i,\max}$ are the lower and upper output limits of the electricity-related energy unit i, respectively; $P_i(t)$ is the output of the electricity-related energy unit i at time t; $H_{i,\min}$ and $H_{i,\max}$ are the lower and upper output limits of the heating-related energy unit i, respectively; $H_i(t)$ is the output of the heating-related energy unit i at time t; $C_{i,\min}$ and $C_{i,\max}$ are the lower and upper output limits of the cooling-related energy unit i, respectively; and $C_i(t)$ is the output of the cooling-related energy unit i at time t.

2) Electricity purchase constraints

$$\begin{cases} 0 \le P_{gb}(t) \le v_b(t) P_{gb,\max} \\ 0 \le P_{gs}(t) \le v_s(t) P_{gs,\max} \end{cases} \tag{22}$$

where P_{gb} and $P_{gb,\max}$ are the purchased power and its upper limit, respectively; $v_b(t)$ and $v_s(t)$ are the power purchasing and power selling states, respectively; and P_{gs} and $P_{gs,\max}$ are the sold power and its upper limit, respectively.

The optimization model, comprising the objective function and constraints described above, represents a deterministic framework. However, the IECPS encounters numerous stochastic factors during actual operation. Therefore, it is essential to incorporate uncertainty effects into the model. Considering the high variability and stochastic nature of RES output and load demand, this study employs the robust interval method to characterize the uncertainty of RES output and load power, specifically addressing day-ahead prediction deviations, as expressed in:

$$\begin{cases} \beta = \bar{\beta} + \Delta\beta \\ \Delta\beta = \xi^{ld}\beta^{ld} + \xi^{ud}\beta^{ud} \end{cases} \tag{23}$$

where β and $\bar{\beta}$ are the actual and predicted values of the uncertain variable, respectively; $\Delta\beta$ is the interval defining the fluctuation bounds of the uncertain variable; β^{ud} and β^{ld} are the upper and lower limits of fluctuation intervals, respectively; and ξ^{ud} and ξ^{ld} are the proportional deviations of the uncertain variable relative to the upper and lower bounds of fluctuation interval, respectively.

Based on (23), the IECPS optimization model that accounts for uncertainty in RES output and load demand is formulated as:

$$\begin{cases} \min\limits_{x \in X} \max\limits_{\beta \in W} F_r(x, \beta) \\ \text{s.t. (SA1), (2), (21), (22)} \end{cases} \tag{24}$$

where x and β are the decision variable and uncertain variable, respectively, with corresponding feasible sets X and W. This model exhibits a typical min-max structure. The dual method is applied to decompose the inner and outer optimization layers. Detailed steps of the decomposition are provided in Supplementary Material B.

The cyber event is defined as:

$$E(type_{cyb})(ID_{cyb})(t_{cyb}, d_{cyb}, s_{cyb}\{s_e, s_h, s_c\}) \tag{25}$$

where $E(type_{cyb})$ is the cyber event index; ID_{cyb} is the cyber node identifier; t_{cyb} and d_{cyb} are the occurrence time and location of cyber event, respectively; and $s_{cyb}\{s_e, s_h, s_c\}$ is the set of multi-dimensional properties of cyber event, and s_e, s_h, and s_c are the operating states of the electricity, heating, and cooling subsystems, respectively. The decision layer performs timeout validation when integrating physical events e_{pc}. Events exceeding the timeout threshold are deemed invalid and discarded.

To regulate energy units in the physical layer, the decision layer transmits the generated cyber events e_{cyb} to control nodes in the integration layer. Control nodes ascertain the acceptance based on location information embedded within cyber events e_{cyb}. For example, a control node associated with the electricity subsystem will discard a cyber event e_{cyb} pertaining to the heating subsystem. The control event e_{con} is defined as:

$$E(type_{con})(ID_{con,k})(t_{con}, d_{con}, s_{con}\{s_1, s_2, ..., s_n\}) \tag{26}$$

where $E(type_{con})$ is the control event index; $ID_{con,k}$ is the control node identifier; t_{con} and d_{con} are the occurrence time and location of control event, respectively; and $s_{con}\{s_1, s_2, ..., s_n\}$ is the set of multi-dimensional properties of control event. The property set includes information regarding the energy units requiring adjustment. The control node performs timeout validation when processing the cyber event e_{cyb}. Events exceeding the timeout threshold are considered invalid and discarded.

Upon receiving the cyber event e_{cyb}, the control node evaluates the cyber event and generates control event e_{con}, which is transmitted to the actuators in the physical layer for execution. This operation is executed by the control function F_{ctr} within the integration layer. For example, the cyber event at this stage can be expressed as:

$$E(type_{cyb})(ID_{cyb})(t_{cyb}, d_{cyb}, s_{cyb}\{1, 2, 0\}) \tag{27}$$

Formula (27) indicates that the electricity subsystem must transmit to state 1, the heating subsystem to state 2, and the cooling system remains in its current state. The control logic implemented by function F_{ctr} is expressed as:

$$\begin{cases} d_{cyb} = d_e, s_e = 1: BS = \{0, P_{bs,c}\}, Grid = \{1, P_g\}, GT = \{1, P_{gt}\} \\ d_{cyb} = d_h, s_h = 2: TS = \{1, H_{ts}\}, GB = \{1, H_{gb}\}, HB = \{1, H_{hb}\} \end{cases} \tag{28}$$

where d_h denotes the event occurs in heating subsystem; H_{ts}, H_{gb}, and H_{hb} are the heat generated by the TS, GB, and HB, respectively; the number 1 in the set TS indicates that the TS is operating in the shutdown state; the number 1 in the sets GB and HB indicate that the GB and HB are operating in the on state; the number 1 in $Grid$ indicates that the IECPS is operating in the power purchasing state, with power P_g exchanged by the IECPS with power grid; and the number 1 in GT indicates that the GT is operating in the on state, with power P_{gt} generated by GT.

In (28), the part preceding the colon in each line indicates the information received by the control node, and the part following the colon indicates the control generated by the control node after receiving the corresponding information, i. e., the control command issued to the energy unit in the physical layer. For instance, the first line reflects that the reception of an electricity subsystem event requests a transition to state 1, and the corresponding command issued by the control node activates the charging mode for the BS with the charging power of $P_{bs,c}$.

The resulting control event is expressed as:

$$\begin{cases} E(type_{con})(ID_{con,e})(t_{con}, d_e, s_{con}\{0, 1, 1\}) & d_{cyb} = d_e \\ E(type_{con})(ID_{con,h})(t_{con}, d_h, s_{con}\{1, 1, 1\}) & d_{cyb} = d_h \end{cases} \tag{29}$$

Finally, the control node forwards the control event e_{con} to the physical-layer actuators which regulate the designated energy units according to the information embedded in the control event e_{con}.

The stability analysis of the proposed HA-based modeling method is presented in Supplementary Material C.

IV. Case Studies

A. Parameter Description

An IECPS for simulation analysis is constructed to validate the proposed HA-based modeling method, as illustrated in Fig. 1. The IECPS comprises three subsystems: electricity, heating, and cooling subsystems, as depicted in Fig. 11. The electricity subsystem contains sensor nodes 1 and 2 (managed by sink node 1) and actuator node 1 (managed by control node 1). The heating subsystem includes sensor node 3, sink node 2, actuator node 2, and control node 2. The cooling subsystem consists of sensor node 4, sink node 3, actuator node 3, and control node 3. Each sensor node is equipped with multiple sensors. A decision node generates global objectives for the entire system.

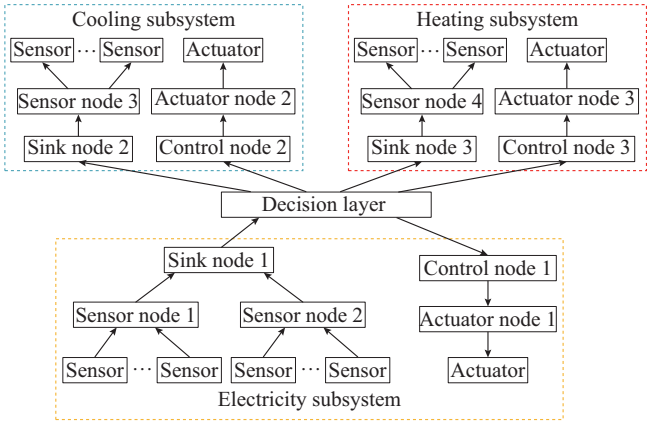

Fig. 11. IECPS for simulation analysis.

Device parameters used in the numerical simulations are detailed in Tables I and II, where the parameter explanations can be found in [27].

TABLE I
PARAMETERS FOR ENERGY UNITS

Parameter	Value	Parameter	Value
η_{gt}	0.6	$P_{cs,\max}$	200 kW
η_{gb}	0.85	$H_{gb,\max}$	1000 kW
$P_{bs,\max}$	150 kW	$C_{ac,\max}$	800 kW
$P_{ts,\max}$	200 kW	$C_{ec,\max}$	650 kW
$P_{gb,\max}$	800 kW	$P_{pv,\max}$	150 kW
$P_{gs,\max}$	800 kW	$P_{gt,\max}$	1200 kW

TABLE II
PARAMETERS FOR ESUS

Unit	$\eta_{i,c}$	$\eta_{i,d}$	δ_i	$E_{i,\min}$ (kWh)	$E_{i,\max}$ (kWh)
BS	0.95	0.95	0.02	300	1350
TS	0.96	0.96	0.01	250	1200
CS	0.96	0.96	0.01	250	1200

B. Results and Discussion

1) Case 1: Comparison with Mixed-integer Programming (MIP) Method

This case evaluates the minimum daily operating cost of IECPS, using the MIP method [32] as a benchmark against the proposed HA-based modeling method. Electricity, heating, and cooling load data, along with renewable energy outputs for a specific day, are employed in the simulation [27], as shown in Supplementary Material D Fig. SD1. Figure 12 presents the optimal output power of energy unit under the MIP method and proposed HA-based modeling method.

As illustrated in Fig. 12, both methods achieve economically efficient system operation, with similar operating states of each energy unit over time. Renewable energy output is assumed to incur zero cost; thus, PV and WT outputs are prioritized to meet electricity load demand at all time. For remaining electricity demand, the grid power is primarily used between 23:00 and 07:00 due to lower prices compared with GT generation costs. Any shortfall is supplemented by GT. During peak price periods from 08:00 to 11:00 and 19:00 to 22:00, the BS in the discharging state and GT supply the remaining load. Surplus electricity is sold to the grid, generating additional revenue.

For the heating load, during low-price periods, heat is supplied by the HB through waste heat recovery from GT generation, with shortfall supplied by the GB. During peak- and flat-price periods, the heating load is primarily satisfied by the HB due to the higher output power of GT. Recycling waste heat via the GB improves the economic performance of IECPS. At this time, the GB remains off, while the surplus heat is stored in the TS. The TS operates in the heat release mode to supply thermal load during heat-deficit periods.

For the cooling load, during the low-price period, EC dominates the supply. During the peak- and flat-price periods, the cooling load is mainly supplied by the AC, with shortfall supplied by the EC. The CS operates in the cooling storage mode during periods with surplus cooling energy and switches to cooling release mode to meet demand during periods with deficit cooling energy.

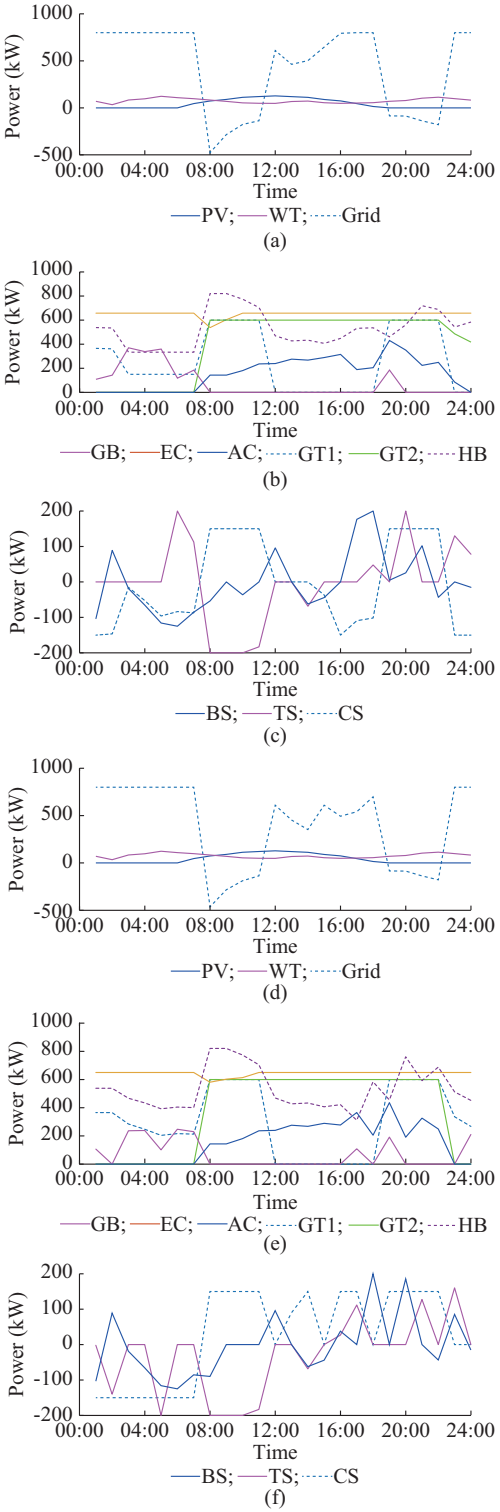

Fig. 12. Optimal output power of energy unit. (a) EPU under MIP method. (b) ECU under MIP method. (c) ESU under MIP method. (d) EPU under proposed HA-based modeling method. (e) ECU under proposed HA-based modeling method. (f) ESU under proposed HA-based modeling method.

The operating states of energy units under both methods are presented in Supplementary Material D Fig. SD3. To assess the impact of robust interval selection on optimization results, simulations are conducted with varying the conservatism parameter. The operating costs of IECPS are summa-

rized in Table III.

TABLE III
OPERATING COSTS OF IECPS UNDER DIFFERENT Γ

Γ	Operating cost (¥)
0	26032
2	28886
4	30195
7	33988
10	37042
12	39207

In Table III, $\Gamma=0$ corresponds to the deterministic optimization without considering uncertainties in renewable energy and load, equivalent to Case 1. Table III indicates that the operation costs increase with Γ. This trend indicates that greater consideration of uncertainties in day-ahead scheduling leads to more conservative operation schemes. While the operation costs increase, the robustness of the optimization decision improves, reducing associated risks. Therefore, setting the parameter Γ requires balancing the economic cost against decision risk to achieve an optimal trade-off.

2) Case 2: Comparison with Energy Hub-based Modeling Method

In the context of rapid fluctuations in renewable energy output, the WT output is used as an example to compare the output variability of GT and GB under the proposed HA-based modeling method and the traditional energy hub-based modeling method [33]. The output power curves of WT, GT, and GB are presented in Fig. 13.

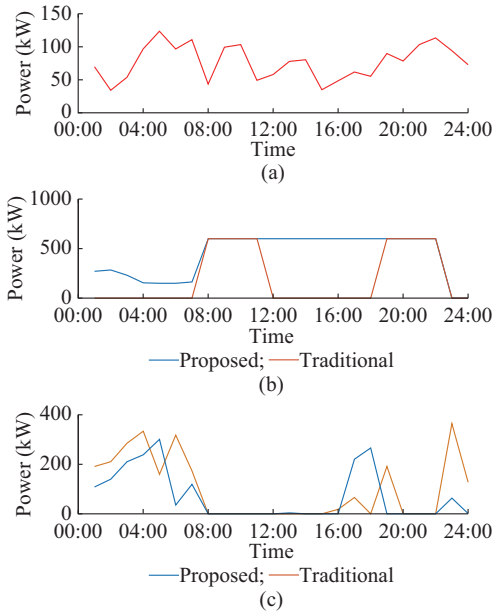

Fig. 13. Output power curves of WT, GT, and GB. (a) WT. (b) GT. (c) GB.

The standard deviation σ quantifies the output fluctuation and serves as the indicator for analyzing the variability of energy unit output. The standard deviation is calculated as:

$$\sigma=\sqrt{\sum_{t=1}^{T}(P_t-P_{ave})^2/T} \tag{30}$$

where P_t is the output power of energy unit at time t; and P_{ave} is the average output power over the optimization period.

Using this formula, the standard deviation of GT and GB outputs under the proposed HA-based modeling method and traditional energy hub-based modeling method are calculated and summarized in Table IV.

TABLE IV
STANDARD DEVIATION OF GT AND GB OUTPUTS

Energy unit	Standard deviation σ	
	Proposed	Traditional
GT	222.9	282.8
GB	100.1	124.7

The data in Table IV indicate that the standard deviation of GT and GB outputs under the traditional energy hub-based modeling method is higher when responding to rapid WT output fluctuations. This corresponds to larger output power variability, as reflected in the output power curves of GT and GB in Fig. 13. By contrast, the proposed HA-based modeling method reduces the standard deviation of GT and GB outputs, indicating improved stability throughout the optimization period. This stability effectively reduces mechanical wear on the energy units, potentially extending their service life. The improved stability under the proposed HA-based modeling method arises from the HA-based state transition model. This model explicitly defines the operating states and transition logic at each stage, enabling each energy unit to respond promptly to rapid WT fluctuations by triggering appropriate state transitions. The enhanced coordination among energy units facilitates power balance, thereby reducing the output power fluctuations.

3) Case 3: Comparative Analysis Under Various Modeling Methods

This study proposes an IECPS event model integrating both temporal and spatial properties. To demonstrate the superiority of this model, three modeling methods are established for comparison:

1) Method 1: the proposed HA-based modeling method considering both temporal and spatial attributes.

2) Method 2: the modeling method considering only temporal attributes.

3) Method 3: the modeling method considering only spatial attributes.

Simulation data from 07:00 to 11:00 are analyzed. The optimization results for the three modeling methods are presented in Supplementary Material D Figs. SD4-6, respectively, which indicate that the output power curves of each energy unit are similar across the three methods. This similarity suggests that all the modeling methods can regulate the output power of energy units based on electricity price information with the goal of minimizing operation costs. However, the differences occur in the operating states of energy units at specific time points. These discrepancies arise because ne-

glecting either spatial or temporal attributes causes actuators to execute incorrect commands.

Daily operating costs of IECPS under Methods 1-3 are ¥26032, ¥26898, and ¥26539, respectively. Method 1 yields the lowest daily operation cost, confirming that integrating both temporal and spatial attributes reduces system expenses. Method 2 shows higher daily operation costs than Method 1. Considering only temporal attributes causes the control node to receive all cyber events e_{cyb} from the decision node indiscriminately. This results in actuators mistakenly executing commands, as shown in Supplementary Material D Fig. SD5(d) and (f), where the heating and cooling subsystems switch to state 2 unnecessarily, increasing the operation costs.

Similarly, Method 3 also exhibits higher operating costs than Method 1. Ignoring temporal attributes leads to delayed event judgment. Sink and control nodes receive outdated events due to network failures or congestion, generating numerous invalid events. This impairs system judgment and causes actuators to execute incorrect commands, thus elevating operating costs.

4) Case 4: Stability Analysis Under Different Methods

1) Load variation

Using the electricity subsystem as an example, the system stability is compared under the proposed HA-based modeling method and the previous method without HA [34] during fluctuations in new energy output and load power changes. Frequency serves as the stability indicator. Simulation results are presented in Supplementary Material D Fig. SD7, which shows that both methods can maintain the system power balance. However, the proposed HA-based modeling method demonstrates superior frequency performance, as shown in Fig. SD7(e). At $t=3$ s and $t=5$ s, when sudden load changes occur, the frequency under the previous method decreases more substantially and recovers to the rated value more gradually. This behavior results from multiple operating states with complex logical relationships. Effective control strategies need to describe the transition logic among these states to allow coordinated switching of energy units. The previous method lacks defined state transition relations, delaying power balance restoration and causing a significant frequency drop. In contrast, the proposed HA-based modeling method defines all operating states and transition conditions, enabling coordinated logic switching and continuous dynamic adjustment. This allows each energy unit to respond rapidly to load changes, reducing frequency deviations.

2) Short-circuit fault

Initially, the wind power is 50 kW, the PV power is 40 kW, and the load is 110 kW. To maintain the power balance, the BS discharges at 22 kW. At $t=0.5$ s, a single-phase short-circuit fault occurs at the user bus and is cleared at $t=0.6$ s. Simulation results under the proposed HA-based modeling method and the previous method without HA are shown in Supplementary Material D Figs. SD8 and SD9, respectively, which reveal that the previous method exhibits larger frequency deviations during the fault, with oscillations in frequency and energy unit outputs after the fault clearance. The proposed HA-based modeling method produces smaller frequency deviations and enables rapid restoration to stable operation following fault clearance. These results confirm the improved frequency stability of the proposed HA-based modeling method under load variation and short-circuit fault conditions compared with the previous method.

V. Conclusion

This paper proposes an HA-based spatial-temporal event modeling method for IECPS. The feasibility of this method is demonstrated through case studies. The main conclusions are as follows.

1) Compared with the traditional energy hub-based modeling methods, CPS reduces system operating costs by enabling real-time monitoring of the operating state.

2) The spatial-temporal modeling method for IECPS outperforms the methods considering only temporal or spatial attributes, enabling more precise regulation of the IECPS.

The spatial-temporal event modeling method offers theoretical guidance for applying CPS in the optimal operation of IECPS. System robustness can be enhanced by deploying multiple sensors and actuator nodes. Future research will address time delays, cyberattacks, missing data, noise, and other practical challenges. Additionally, the current model considers only the active power of WTs and GTs. Neglecting reactive power may reduce accuracy under certain conditions. Future work will incorporate reactive power effects to improve model fidelity.

References

[1] J. Li, Z. Fang, Q. Wang *et al*., "Optimal operation with dynamic partitioning strategy for centralized shared energy storage station with integration of large-scale renewable energy," *Journal of Modern Power Systems and Clean Energy*, vol. 12, no. 2, pp. 359-370, Mar. 2024.

[2] C. Wang, M. Wang, A. Wang *et al*., "Multiagent deep reinforcement learning-based cooperative optimal operation with strong scalability for residential microgrid clusters," *Energy*, vol. 314, p. 134165, Jan. 2025.

[3] Y. Yang, P. Yang, Z. Zhao *et al*., "An adaptive optimal scheduling strategy for islanded micro-energy grid considering the multiple system operating states," *IEEE Transactions on Sustainable Energy*, vol. 14, no. 1, pp. 393-408, Jan. 2023.

[4] W. Kong, K. Sun, and J. Zhao, "Two-stage optimal scheduling of community integrated energy system considering operation sequences of hydrogen energy storage systems," *Journal of Modern Power Systems and Clean Energy*, vol. 13, no. 1, pp. 276-288, Jan. 2025.

[5] Z. Wang, J. Wang, X. Duan *et al*., "A coordinator-event-axis-based time synchronization strategy for cyber-physical power system co-simulation," *IEEE Transactions on Smart Grid*, vol. 15, no. 4, pp. 4090-4103, Jul. 2024.

[6] Y. Yang, P. Zhang, C. Wang *et al*., "State transition modeling method for optimal dispatching for integrated energy system based on cyber-physical system," *Journal of Modern Power Systems and Clean Energy*, vol. 12, no. 5, pp. 1617-1630, Sept. 2024.

[7] H. Fan, Y. Sheng, E. Lu *et al*., "Integrated energy cyber-physical system fusion modeling and operation state analysis under the cooperative attack," *Electric Power Systems Research*, vol. 234, p. 110466, Sept. 2024.

[8] D. Liu, Q. Zhang, H. Liang *et al*., "Modeling and analysis of risk propagation and loss causing capacity for key nodes in cyber-physical coupled power network," *Complex System Modeling and Simulation*, vol. 4, no. 2, pp. 124-136, Jun. 2024.

[9] Z. Yang, Y. Xiang, K. Liao *et al*., "Research on security defense of coupled transportation and cyber-physical power system based on the static Bayesian game," *IEEE Transactions on Intelligent Transportation Systems*, vol. 24, no. 3, pp. 3571-3583, Mar. 2023.

[10] L. Chen and B. Wang, "Robustness assessment of weakly coupled cyber-physical power systems under multi-stage attacks," *Electric Power Systems Research*, vol. 231, p. 110325, Jun. 2024.

[11] H. Zhu, B. Xia, D. Zhou *et al*., "Research on integrated model and interactive influence of energy Internet cyber physical system," in *Proceedings of 2020 IEEE Sustainable Power and Energy Conference*, Chengdu, China, Nov. 2020, pp.1667-1671.
[12] K. Zhao, Y. Wang, J. Kou *et al*., "Integrated energy information physical system model and its simulation control," in *Proceedings of 2020 International Conference on Communications*, *Information System and Computer Engineering*, Kuala Lumpur, Malaysia, Jul. 2020, pp. 173-177.
[13] S. Soleimani, A. Afshar, and H. Atrianfar, "Critical component analysis of cyber-physical power systems in cascading failures using graph convolutional networks: an energy-based approach," *Sustainable Energy*, *Grids and Networks*, vol. 42, p. 101653, Jun. 2025.
[14] M. Gholami, A. Gholami, and M. Mohammadtaheri, "Cyber-physical power system reliability assessment considering multi-state independent components," *Electric Power Systems Research*, vol. 217, p. 109141, Apr. 2023.
[15] J. Haack, A. Narayan, A. D. Patil *et al*., "A hybrid model for analysing disturbance propagation in cyber-physical energy systems," *Electric Power Systems Research*, vol. 212, p. 108356, Nov. 2022.
[16] Z. S. Li, G. Wu, R. Cassandro *et al*., "A review of resilience metrics and modeling methods for cyber-physical power systems (CPPS)," *IEEE Transactions on Reliability*, vol. 73, no. 1, pp. 59-66, Mar. 2024.
[17] X. Kong, Z. Lu, X. Guo *et al*., "Resilience evaluation of cyber-physical power system considering cyber attacks," *IEEE Transactions on Reliability*, vol. 73, no. 1, pp. 245-256, Mar. 2024.
[18] X. Sun, J. Chen, and Q. Xu, "Sequential post-disaster recovery strategy for cyber physical energy systems considering electric-gas coupling characteristics," in *Proceedings of 2024 IEEE 19th Conference on Industrial Electronics and Applications*, Kristiansand, Norway, Aug. 2024, pp. 1-5.
[19] C. Konstantinou and O. M. Anubi, "Resilient cyber-physical energy systems using prior information based on Gaussian process," *IEEE Transactions on Industrial Informatics*, vol. 18, no. 3, pp. 2160-2168, Mar. 2022.
[20] Y. Zhang, M. Fei, Q. Sun *et al*., "A multi-objective and multi-constraint optimization model for cyber-physical power systems considering renewable energy and electric vehicles," *IEEE/CAA Journal of Automatica Sinica*, vol. 10, no. 6, pp. 1498-1500, Jun. 2023.
[21] M. Barani and V. V. Vadlamudi, "Analytical approach for adequacy assessment of cyber-physical multi-microgrid distribution systems with distributed generation," *Electric Power Systems Research*, vol. 212, p. 108293, Nov. 2022.
[22] D. Ding, J. Li, H. Wang *et al*., "Short-term load forecasting reliability in power plant of cyber-physical energy system considering adaptive denoising," *IEEE Systems Journal*, vol. 17, no. 4, pp. 5183-5194, Dec. 2023.
[23] W. Dai, C. Pang, V. Vyatkin *et al*., "Discrete-event-based deterministic execution semantics with timestamps for industrial cyber-physical systems," *IEEE Transactions on Systems*, *Man*, *and Cybernetics*: *Systems*, vol. 50, no. 3, pp. 851-862, Mar. 2020.
[24] G. Liao, X. Huang, N. Xiong *et al*., "Softwarized attention-based context-aware group recommendation technology in event-based industrial cyber-physical systems," *IEEE Transactions on Industrial Informatics*, vol. 17, no. 10, pp. 6894-6905, Oct. 2021.
[25] Y. Wang, T. L. Nguyen, Y. Xu *et al*., "Cyber-physical design and implementation of distributed event-triggered secondary control in islanded microgrids," *IEEE Transactions on Industry Applications*, vol. 55, no. 6, pp. 5631-5642, Nov.-Dec.2019.
[26] M. Z. A. Bhuiyan, J. Wu, G. Wang *et al*., "Sensing and decision making in cyber-physical systems: the case of structural event monitoring," *IEEE Transactions on Industrial Informatics*, vol. 12, no. 6, pp. 2103-2114, Dec. 2016.
[27] Y. Yang, P. Yang, Z. Zhao *et al*., "A multi-timescale coordinated optimization framework for economic dispatch of micro-energy grid considering prediction error," *IEEE Transactions on Power Systems*, vol. 39, no. 2, pp. 3211-3226, Mar. 2024.
[28] C. Dou, S. Teng, T. Zhang *et al*., "Event-triggered hybrid control strategy based on hybrid automata and decision tree for microgrid," *IET Generation*, *Transmission & Distribution*, vol. 13, no. 14, pp. 3066-3077, Jul. 2019.
[29] W. Zhang, S. Tan, S. Chen *et al*., "Visual reasoning for uncertainty in spatio-temporal events of historical figures," *IEEE Transactions on Visualization and Computer Graphics*, vol. 29, no. 6, pp. 3009-3023, Jun. 2023.
[30] B. B. Batu, T. T. Temizel, and H. Ş. Düzgün, "A non-parametric algorithm for discovering triggering patterns of spatio-temporal event types," *IEEE Transactions on Knowledge and Data Engineering*, vol. 29, no. 12, pp. 2629-2642, Dec. 2017.
[31] Y. Huang, L. Zhang, and P. Zhang, "A framework for mining sequential patterns from spatio-temporal event data sets," *IEEE Transactions on Knowledge and Data Engineering*, vol. 20, no. 4, pp. 433-448, Apr. 2008.
[32] Z. Deng, M. Liu, H. Chen *et al*., "Optimal scheduling of active distribution networks with limited switching operations using mixed-integer dynamic optimization," *IEEE Transactions on Smart Grid*, vol. 10, no. 4, pp. 4221-4234, Jul. 2019.
[33] Y. Luo, X. Xu, Z. Zhang *et al*., "A two-stage robust scheduling optimization of an energy hub with multiple chance constraints," in *Proceedings of 2023 IEEE/IAS Industrial and Commercial Power System Asia*, Chongqing, China, Jul. 2023, pp. 650-655.
[34] T. Heins, M. Joševski, S. K. Gurumurthy *et al*., "Centralized model predictive control for transient frequency control in islanded inverter-based microgrids," *IEEE Transactions on Power Systems*, vol. 38, no. 3, pp. 2641-2652, May 2023.

Yi Yang received the B.S. degree in electrical engineering from Yangtze University, Jingzhou, China, in 2015, the M.S. degree in electrical engineering from Hunan University, Changsha, China, in 2018, and the Ph.D. degree in electrical engineering from South China University of Technology, Guangzhou, China, in 2023. He is currently a Lecturer with the College of Electrical Engineering and New Energy, China Three Gorges University, Yichang, China. His research interests include power electronics for microgrid, integrated energy system optimization, and power cyber-physical system.

Ping Tang received the B.S. degree in electrical engineering from Hunan University of Technology, Zhuzhou, China in 2024. He is currently pursuing the master's degree in the College of Electrical Engineering and New Energy, China Three Gorges University, Yichang, China. His research interests include integrated energy system optimization and power cyber-physical system.

Can Wang received the B.S. and M.S. degrees in control theory and engineering from Wuhan University of Science and Technology, Wuhan, China, in 2010 and 2013, respectively, and the Ph.D. degree in electrical engineering from South China University of Technology, Guangzhou, China, in 2017. He is currently an Associate Professor of Electrical Engineering with the College of Electrical Engineering and New Energy, China Three Gorges University, Yichang, China. His current research interests include distributed generation, microgrid operation and control, integrated energy system, and smart grid.

Nan Yang received the B.S. degree in electrical engineering from Taiyuan University of Technology, Taiyuan, China, in 2009, and the Ph.D. degree in electrical engineering from Wuhan University, Wuhan, China, in 2014. From 2019 to 2020, he worked as a Visiting Scholar with the Stevens Institute of Technology, Hoboken, USA. He is currently a Professor at the College of Electrical Engineering and New Energy, China Three Gorges University, Yichang, China. His research interests include power dispatching automation of new energy source, artificial intelligence, planning and operation of power system, microgrid operation and control, and active distribution network.

Zhuoli Zhao received the Ph.D. degree in electrical engineering from South China University of Technology, Guangzhou, China, in 2017. He is currently an Associate Professor with the School of Automation, Guangdong University of Technology, Guangzhou, China. His research interests include microgrid control and energy management, renewable power generation control and grid-connected operation, modeling, analysis and control of power-electronized power system and smart grid.